

Photodissociation dynamics of CO₂ at 157.6 nm by photofragment-translational spectroscopy

Albert Stolow^{a)} and Yuan T. Lee

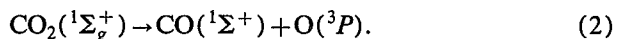
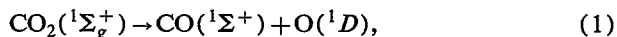
Department of Chemistry, University of California and Chemical Sciences Division, Lawrence Berkeley Laboratory, Berkeley, California 94720

(Received 30 July 1992; accepted 20 October 1992)

The photodissociation of CO₂ at 157 nm was studied by the photofragment-translational spectroscopy technique. Product time-of-flight spectra were recorded and center-of-mass translational energy distributions were determined. Two electronic channels were observed—one forming O(¹D) and the other O(³P). With previously determined anisotropy parameters of $\beta=2$ for the O(³P) channel and $\beta=0$ for the O(¹D) channel, an electronic branching ratio of $6\% \pm 2\%$ O(³P) was obtained, consistent with previous results. The translational energy distribution for the CO(ν) + O(³P) channel was very broad (over 30 kcal/mol) and appeared to peak near CO($\nu=0$). The value of $\beta=2$ for the O(³P) channel was confirmed by comparing Doppler profiles, derived from our measured translational energy distribution, with previously measured Doppler profiles. This suggests that the O(³P) channel arises from a direct transition to an excited triplet state. The O(¹D) channel had a structured time-of-flight which related to rovibrational distributions of the CO product. The influence of the excitation of the CO₂(ν_2) bending mode was investigated and shown to have a small but not negligible contribution. Based upon a comparison of our data with a previous vacuum-ultraviolet (VUV) laser induced fluorescence study, we obtain as our best estimate of the vibrational branching ratio, CO($\nu=0$)/CO($\nu=1$) = 1.9, for the CO(ν) + O(¹D) channel.

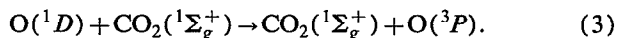
INTRODUCTION

The vacuum-ultraviolet (VUV) photochemistry of CO₂ is an intriguing and important problem. Not only is CO₂ an important atmospheric constituent, but its relative simplicity should allow for detailed study and comparison with theory. For wavelengths in the range 140–170 nm, CO₂ dissociation has two open channels,



The latter channel, reaction (2), represents a spin-forbidden process.

Earlier work¹ in a gas bulb indicated that the quantum yield for reaction (1) is unity at 131 and 147 nm, consistent with the expectation that a spin-forbidden process should be very unfavorable in a triatomic molecule consisting of carbon and oxygen atoms (i.e., relatively small spin-orbit coupling). Although O(³P) was observed, it could be completely accounted for via collisional relaxation of O(¹D),



It is well known that O(¹D) is quenched by atmospheric molecules² with near gas kinetic efficiency. The weak spin-orbit coupling, however, suggests that such processes should be inefficient in simple encounters: The observed high quenching efficiency arises from the formation of a long-lived complex (i.e., several vibrational periods), in-

creasing the probability of spin transition via multiple crossings of the singlet-triplet intersection region.

Recently, the photolysis of CO₂ at 157 nm was investigated using a chemical scavenging technique.³ It was suggested that the primary photoprocess producing O(³P) [reaction (2)] contributes about 6% to the quantum yield. A subsequent study of the O(³P, $j''=2,1,0$) state distribution and Doppler profiles in a molecular beam experiment⁴ confirmed the primary character of this channel. The Doppler profiles were analyzed to give an anisotropy parameter of $\beta=2$. A β value of two is usually expected for a very direct dissociation from a linear excited state wherein the recoil velocity vector is parallel to the electronic transition moment vector.

Most recently, the vibrational and rotational distributions of the CO(¹ Σ^+) product were measured in a pump-and-probe experiment via VUV (vacuum ultraviolet) laser induced fluorescence.⁵ The CO product was found to have a highly excited rotational distribution, terminating abruptly at the energetic limit. This is indicative of dissociation occurring from a bent excited state. Consistent with this was a measurement of an anisotropy parameter of $\beta=0$, corroborating the suggestion that the excited state is bent. If the molecule bends strongly as it dissociates, the recoil velocity vector will be at a large angle relative to the transition moment vector and, hence, the β parameter will be small.

The excited states of CO₂ are very complicated.⁶ There are two weak bands between the CO₂(¹ Σ_g^+) ground state and the group of {¹ Π_g , ¹ Σ_u^- , ¹ Δ_u , and ¹ Σ_g^+ } excited states that occur in the range 120–200 nm and all are electric dipole forbidden ($D_{\infty h}$ symmetry). The electronic transition, however, can be vibronically induced by a bending vibration. The first band, beginning around 6 eV with a

^{a)}Present address: Ultrafast Phenomena Group, Steacie Institute for Molecular Sciences, National Research Council of Canada, Ottawa, Canada.

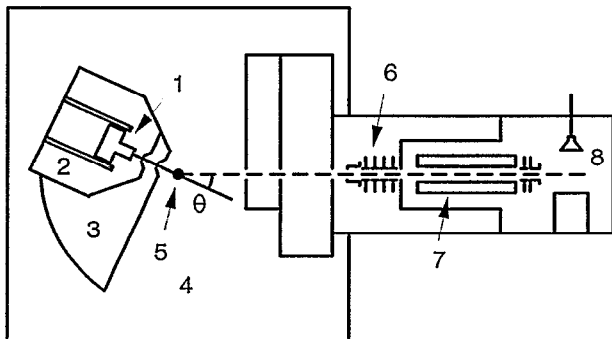


FIG. 1. A schematic drawing of the photofragment spectrometer. (1) heated molecular beam nozzle, (2) source chamber, (3) differential chamber, (4) main chamber, (5) laser interaction point, (6) ionizer, (7) quadrupole mass spectrometer, (8) detector.

maximum near 8.4 eV, is irregular and diffuse and no assignments have been made. Excitation at 157 nm corresponds to this transition. At higher energy, the second transition is sharper and more regular, peaking near 9.3 eV. The first optically allowed transition appears around 11.1 eV. High accuracy electronic structure calculations⁷ for CO₂ have been performed in the Franck-Condon region (i.e., linear $D_{\infty h}$ structures) for the lowest singlet excited states: ${}^1\Pi_g$, ${}^1\Sigma_u^-$, and ${}^1\Delta_u$. It was shown that in the Franck-Condon region between 120 and 170 nm, the nearly overlapping ${}^1\Delta_u$ and ${}^1\Sigma_u^-$ states are involved in conical intersections with the ${}^1\Pi_g$ state. (This most likely explains the irregular, unresolved structure in the first absorption band.) Thus, the photophysics of CO₂ is very complex and cannot be described within the Born-Oppenheimer approximation. Along the bending coordinate, the electronically degenerate ${}^1\Pi_g$ and ${}^1\Delta_u$ states split into Renner-Teller pairs of 1A_2 and 1B_2 symmetry. These are strongly stabilized by bending, as is the nondegenerate ${}^1\Sigma_u^-$ state. The bent 1B_2 component of the ${}^1\Delta_u$ state has been analyzed (i.e., the carbon monoxide flame bands⁸) and the OCO bond angle was found to be 122°—very strongly bent.

In this study, we employ the technique of photofragment-translational spectroscopy to study the photodissociation dynamics of CO₂ at 157 nm in a molecular beam. The existence of the O(³P) channel further suggests that triplet surfaces must also be involved in the dissociation dynamics. The excited states are calculated to be strongly bent and this feature should be revealed in the product state distributions.

EXPERIMENT

The high resolution rotating source photofragment-translation spectrometer has been described previously in detail.⁹ A brief description follows; a schematic drawing of the apparatus is shown in Fig. 1. A molecular beam is formed by passing gas through a heatable nozzle, (1) into a source chamber (2), where it was skimmed, passed into a differential chamber (3), skimmed again and finally passed into the main interaction chamber (4). A pulsed

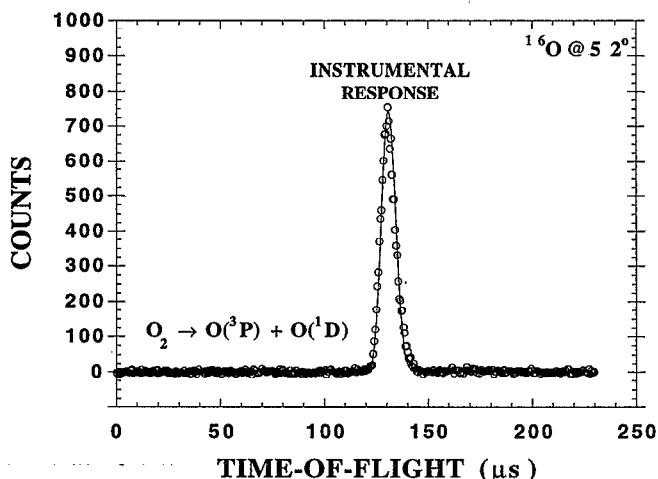


FIG. 2. A time-of-flight distribution for O₂ photodissociation at 157 nm. At a lab frame angle of 52° (perpendicular to the molecular beam velocity vector in the center-of-mass frame) the narrow, single kinetic energy release peak serves to determine the instrumental response function which was used in all subsequent convolutions.

laser crosses the molecular beam at (5), which is also the viewing axis of the triply differentially pumped quadrupole mass spectrometer. Time-of-flight spectra are obtained by recording the distribution of arrival times of photodissociation product molecules at the detector. Angular distributions are obtained by rotating the molecular beam about the point (5).

In high resolution photofragment-translational energy spectroscopy, it is important to determine the instrumental response function (i.e., the time response of the instrument to a δ -function input). This is best done by dissociating a diatomic molecule. In this case, we chose O₂ which absorbs well at 157 nm and has a unit quantum yield for dissociation into O(¹D) + O(³P) at this wavelength.¹⁰ This channel has a single kinetic energy release of 18.84 kcal/mol. A seeded mixture of 0.5% O₂ in He was expanded through a 175 μ m nozzle (at 105 °C) and determined to have a lab velocity of 1.69×10^5 cm/s with a speed ratio of 13.3. It is important to reduce the effect of this small spread in beam velocities on the determination of the instrumental response function. We chose, therefore, the lab frame detection angle which was perpendicular to the molecular beam velocity vector in the center-of-mass frame. For O₂ photodissociation at 157 nm and a beam velocity of 1.69×10^5 cm/s, this corresponds to a lab frame detection angle of 52°. In Fig. 2, we show a time-of-flight (TOF) spectrum for O atom recoil at a lab angle of 52°. The narrow peak serves to determine the instrumental response function (i.e., the ionizer width) which was subsequently used in the analysis of the CO₂ photodissociation data.

In an ultrahigh vacuum chamber, such as the detector of the present apparatus, the most abundant background gases are typically H₂ and CO which evolve naturally from stainless steel. This means that the detection of CO⁺ ($m/e=28$), O⁺ ($m/e=16$), and C⁺ ($m/e=12$) in a photofragmentation experiment is quite difficult. Although we

did a considerable amount of signal averaging at $m/e=28$ (e.g., over 10^6 shots) in order to detect ^{12}CO recoil from $^{12}\text{CO}_2$, it was found that the signal-to-noise ratio could be improved by orders of magnitude when using isotopically substituted carbon— $^{13}\text{CO}_2$. In this case, the detected mass is $m/e=29$ and the background signal is very small.

Seeded mixtures of isotopically substituted carbon dioxide (5% $^{13}\text{CO}_2$, 95% He) with a stagnation pressure of 200 torr were expanded through a 175 μm diam nozzle, which was heated to 115 °C. The expansions were typically characterized by a lab velocity of 1.6×10^5 cm/s and a speed ratio of 11. The heated nozzle ensured that no clusters were present. This was checked by looking for parent $^{13}\text{CO}_2$ molecules recoiling from the molecular beam at small angles: If a cluster, $(\text{CO}_2)_n$, was photodissociated, there should be a monomer unit, CO_2 , recoiling from the beam due to fragmentation of the cluster. No evidence of cluster formation was found. The bending frequency of $^{13}\text{CO}_2$ in the ground state is rather low ($\nu_2=654\text{ cm}^{-1}$) and doubly degenerate. Therefore, at room temperature $\text{CO}_2(\nu_2=1)$ constitutes around 8% of the ground state population, whereas at 115 °C, it constitutes about 17%. There may, however, have been some relaxation of this mode during the supersonic expansion.

The 157 nm laser used in this experiment was a Lambda-Physik VUV excimer LPF 205. Specifically optimized for operation at 157 nm, it was capable of producing over 100 mJ/pulse at 50 Hz with a gas lifetime of 300 000 shots. These features proved important in a small-signal experiment such as photofragment-translational spectroscopy. The laser power was continuously monitored during the experiments by a vacuum-adapted Scientech power meter. The beam path between the excimer and the vacuum chamber consisted of a copper tube which was evacuated to approximately 10^{-3} torr. A 2 in. diam, 50 cm f.l. VUV-grade MgF_2 lens (Janos) was used to focus the excimer output to a 3 mm \times 5 mm spot at the interaction region. The copper tube could be isolated and small amounts of air could be leaked in, providing a simple neutral density filter when it was necessary to attenuate the laser.

The 157 nm excimer laser operated at two narrow VUV lines (approximately 1 cm^{-1} bandwidth). The main line (85%) lases at 157.63 nm ($64\,440\text{ cm}^{-1}$ or 181.34 kcal/mol). $D_0(\text{O}^{13}\text{C}\cdots\text{O})$ was taken to be 171.20 kcal/mol for the $\text{O}(^1D)$ channel and 125.88 kcal/mol for the $\text{O}(^3P)$ channel (i.e., corrected for ^{13}C isotopic shifts).¹¹ The available energies for the various fragmentation channels are given in Table I. The Newton diagram illustrating these center-of-mass recoil energies is shown in Fig. 3. The lab angles of 10° and 30° were used most frequently in recording the TOF spectra as these two angles were most sensitive to the slower and faster components, respectively, of the $\text{O}(^1D)$ translational energy distributions. The $\text{O}(^3P)$ channel is better resolved at larger angles (30°).

Time-of-flight spectra consisting of 300 000–1 100 000 co-added shots were recorded. Product center-of-mass translational energy distributions were extracted using the forward convolution technique.⁹

TABLE I. $^{13}\text{CO}_2$ energetics for 157.6 nm photodissociation. The available translational energies of the fragmentation channels for CO_2 dissociation at 157.63 nm. The $\text{O}(^3P)$ and $\text{O}(^1D)$ channels are given, as well as the $\text{O}(^1D)$ channel for dissociation of the hot molecule.

Parent	Product	Energy available
$^{13}\text{CO}_2(\nu_2=0)$	$^{13}\text{CO}(v=0) + \text{O}(^3P)$	55.458 kcal/mol
	$^{13}\text{CO}(v=1) + \text{O}(^3P)$	49.467 kcal/mol
	$^{13}\text{CO}(v=2) + \text{O}(^3P)$	43.548 kcal/mol
	$^{13}\text{CO}(v=3) + \text{O}(^3P)$	37.701 kcal/mol
	$^{13}\text{CO}(v=4) + \text{O}(^3P)$	31.928 kcal/mol
$^{13}\text{CO}_2(\nu_2=0)$	$^{13}\text{CO}(v=0) + \text{O}(^1D)$	10.142 kcal/mol
	$^{13}\text{CO}(v=1) + \text{O}(^1D)$	4.151 kcal/mol
$^{13}\text{CO}_2(\nu_2=1)$	$^{13}\text{CO}(v=0) + \text{O}(^1D)$	12.011 kcal/mol
	$^{13}\text{CO}(v=1) + \text{O}(^1D)$	6.020 kcal/mol
	$^{13}\text{CO}(v=2) + \text{O}(^1D)$	0.101 kcal/mol

RESULTS

Time-of-flight spectra for the ^{13}CO photofragment at lab angles of 10° and 30° are shown in Figs. 4 and 5, respectively. Two channels are clearly identified. The large, structured feature at later times corresponds to the $\text{O}(^1D)$ channel—reaction (1). Definitive evidence for the spin-forbidden $\text{O}(^3P)$ channel—reaction (2)—is seen in the small, fast peak at early times in Figs. 4 and 5. Without making any assumptions about internal energy distributions, these two channels were fit to obtain the overall product translational energy probability distribution function, $P(E)$, for each channel. The best fit $P(E)$ for reaction (1) is shown in Fig. 6. All the features seen in this $P(E)$ are required in order to fit the data at both angles. The best fit $P(E)$ for reaction (2) is shown in Fig. 7. Due to the poor signal-to-noise ratio for this channel and the compression of the peak due to its high lab frame velocity, we were

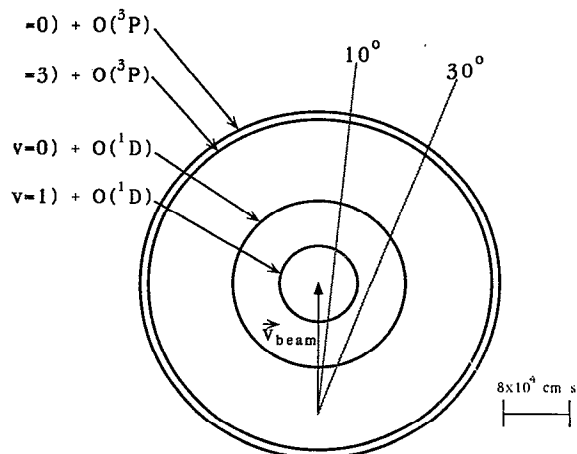


FIG. 3. Newton diagram showing the relationship between lab frame and center-of-mass frame velocities for $\text{CO}_2 \rightarrow \text{CO}(v) + \text{O}(^3P, ^1D)$ at 157 nm. The lab frame velocity of the beam is given by the bold arrow, as indicated. Product CO recoil velocities are shown as circles centered at the tip of the arrow.

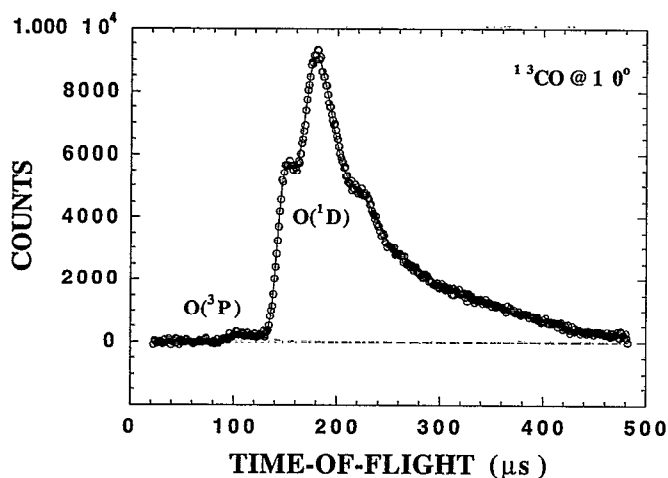


FIG. 4. A time-of-flight distribution at a lab angle of 10° for the ¹³CO fragment from ¹³CO₂ photolysis at 157 nm. The two electronic channels, O(³P) and O(¹D), are indicated. The solid line shows the fit to the O(¹D) channel whereas the dashed line shows the fit to the O(³P) channel.

unable to resolve any structure. It is clear, however, that the ¹³CO product is formed with a broad range of internal energies.

In order to obtain the O(³P)/O(¹D) electronic branching ratio, we preserved the form of each $P(E)$ while varying their ratio so as to best fit the data. We found, as shown in Fig. 8, an O(³P)/O(¹D) electronic branching ratio of $6\% \pm 2\%$, agreeing well with previous results.³ This result was based upon two assumptions. The first is that the anisotropy parameter, β , describing the angular distribution of photoproducts is $\beta=0$ for the O(¹D) channel, as was obtained using the VUV laser induced fluorescence technique.⁵ The second assumption was that $\beta=2$ for the O(³P) channel, based upon Doppler profile measurements on the O(³P) product atom. However, the anal-

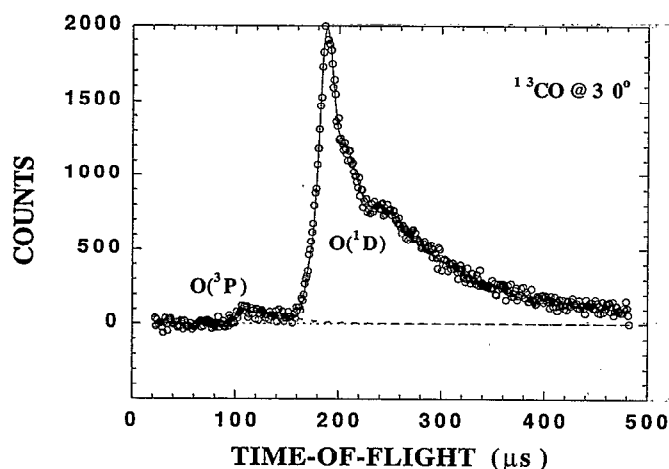


FIG. 5. A time-of-flight distribution at a lab angle of 30° for the ¹³CO fragment from ¹³CO₂ photolysis at 157 nm. The two electronic channels, O(³P) and O(¹D), are indicated. The solid line shows the fit to the O(¹D) channel whereas the dashed line shows the fit to the O(³P) channel.

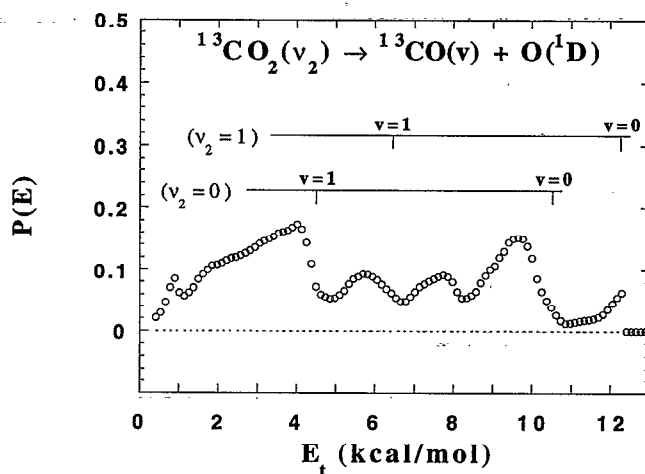


FIG. 6. The translational energy distribution, $P(E)$, for the ¹³CO₂ → ¹³CO(v) + O(¹D) channel used to fit the large feature in Figs. 4 and 5. The thresholds for the formation of CO($v=0$) and CO($v=1$) from both the hot and cold CO₂ molecule are indicated.

ysis which yielded a result of $\beta=2$ rested upon the assumption of a single O(³P) recoil energy. As can be seen from the broad distribution in Fig. 7, this is clearly incorrect. The assumption of $\beta=2$ for the O(³P) channel needs to be further justified. This is discussed in a following section.

In order to confirm the fits to the ¹³CO recoil data of Figs. 4 and 5, we measured product TOF spectra for the ¹⁶O fragment. Due to conservation of momentum in the center-of-mass frame, the ¹³CO $P(E)$ must fit the ¹⁶O atom data without adjustment. This is shown in Fig. 9. Unfortunately, due to the higher background, the signal-to-noise ratio is much worse. Furthermore, the TOF data are contaminated by a feature near 200 μs which does not transform with angle. This is due to the photodissociation of

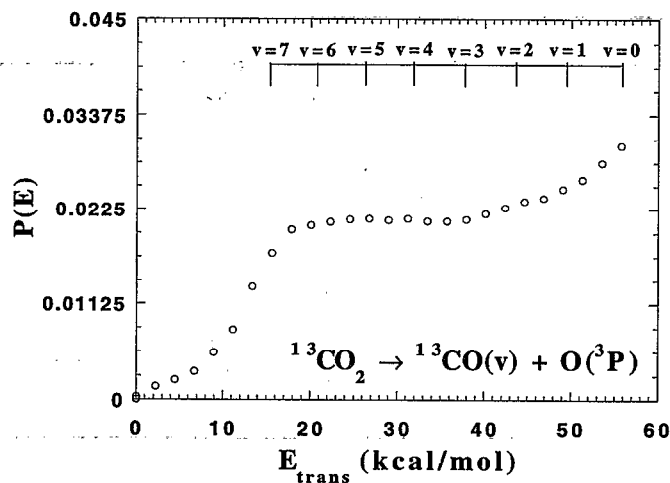


FIG. 7. The translational energy distribution, $P(E)$, for the ¹³CO₂ → ¹³CO(v) + O(³P) channel used to fit the small, fast feature in Figs. 4 and 5. The thresholds for the formation of various CO vibrational states are indicated. It is seen that the distribution of internal energies is very broad.

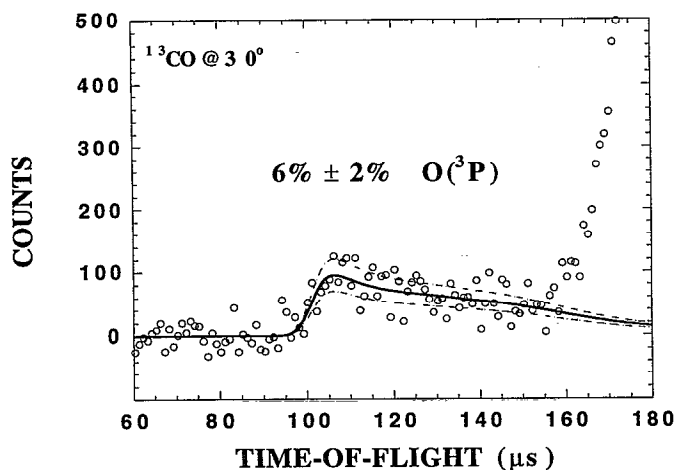


FIG. 8. A time-of-flight distribution at a lab angle of 30° for the ¹³CO fragment from ¹³CO₂ photolysis at 157 nm, showing in greater detail the electronic channel O(³P). The solid line shows the fit to the O(³P) channel using the $P(E)$ of Fig. 7. We estimate the electronic branching ratio to be $6\% \pm 2\%$ O(³P).

background O₂ in the main chamber and is shown clearly (with the molecular beam off) in the middle figure. Once the subtraction of this background is performed, shown in the bottom figure, the momentum matching is satisfactory.

Most experiments described here were carried out using isotopically substituted carbon dioxide—¹³CO₂. However, in order to ensure that isotopic substitution doesn't adversely affect the photodissociation dynamics, we also studied normal ¹²CO₂. The TOF spectra for ¹²CO ($m/e = 28$) recoil are shown in Fig. 10, corresponding to lab detection angles of 20° (top) and 30° (bottom). It can be seen that, despite the poor signal-to-noise ratio, the $P(E)$'s from Figs. 6 and 7 fit the data quite well without adjustment. This indicates that the product translational energy distributions for ¹³CO recoil from ¹³CO₂ and ¹²CO recoil from ¹²CO₂ are quite similar.

In order to avoid the formation of clusters, the nozzle tip was heated to 115 °C during the experiments. Due to the doubly degenerate low frequency bending mode ($\nu_2 = 654 \text{ cm}^{-1}$), there was some hot CO₂ in the molecular beam. In fact, as can be seen in Fig. 6, a small contribution from CO₂($\nu_2 = 1$) dissociation is required to match the leading edge of the O(¹D) peak in Figs. 4 and 5 and to account for the slow shoulder of the O(¹D) peak near 240 μs in Fig. 5. This is discussed further in a subsequent section. To demonstrate the effect of CO₂($\nu_2 = 1$) photodissociation on the TOF data, we measured ¹⁶O recoil from ¹²CO₂ at two disparate temperatures. These are shown in Fig. 11, corresponding to nozzle temperatures of 25 °C (top) and 300 °C (bottom). In the top figure, the data are fit using the $P(E)$ from Fig. 6. The fit is quite good, indicating that the fraction of hot CO₂ in the beam has not decreased much as compared with 115 °C. The leading edge corresponds to the formation of CO($v=0, J$) from CO₂($\nu_2=1$), whereas the small peak near 150 μs corresponds to the formation of CO($v=1, J$) from CO₂($\nu_2=1$).

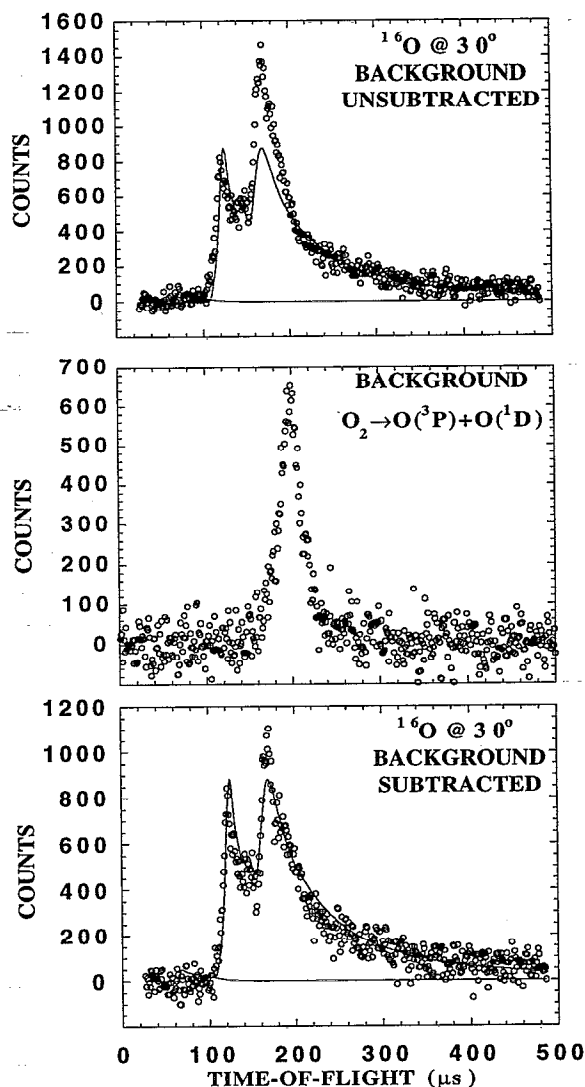


FIG. 9. (top) A time-of-flight spectrum for the ¹⁶O recoil partner at a lab angle of 30°. The data are contaminated by a background peak near 200 μs. (middle) A time-of-flight spectrum showing the ¹⁶O background with the molecular beam off, due to O₂ → O(³P) + O(¹D) in the main chamber. This signal is independent of angle. (bottom). A time-of-flight spectrum for the ¹⁶O recoil partner at a lab angle of 30° with the background subtracted. The momentum matching is good, confirming the accuracy of the $P(E)$ in Fig. 6.

When the nozzle temperature is increased to 300 °C, shown in the bottom of Fig. 11, the fit is not as good. It can be seen that the leading edge of the data is now too fast and that the small peak near 150 μs appears too small. This is consistent with greater concentrations of CO₂($\nu_2 = 1$) in the expanded beam. We suspect that there is significant relaxation of the hot molecule in the beam expansion. As the excited state is strongly bent, the Franck-Condon factors for CO₂($\nu_2 = 1$) should be much greater than for CO₂($\nu_2 = 0$) and, therefore, the former should contribute disproportionately to the TOF data. As can be seen, this contribution is small and therefore we suggest that the concentration of CO₂($\nu_2 = 1$) in the fully expanded beam is minimal but not negligible.

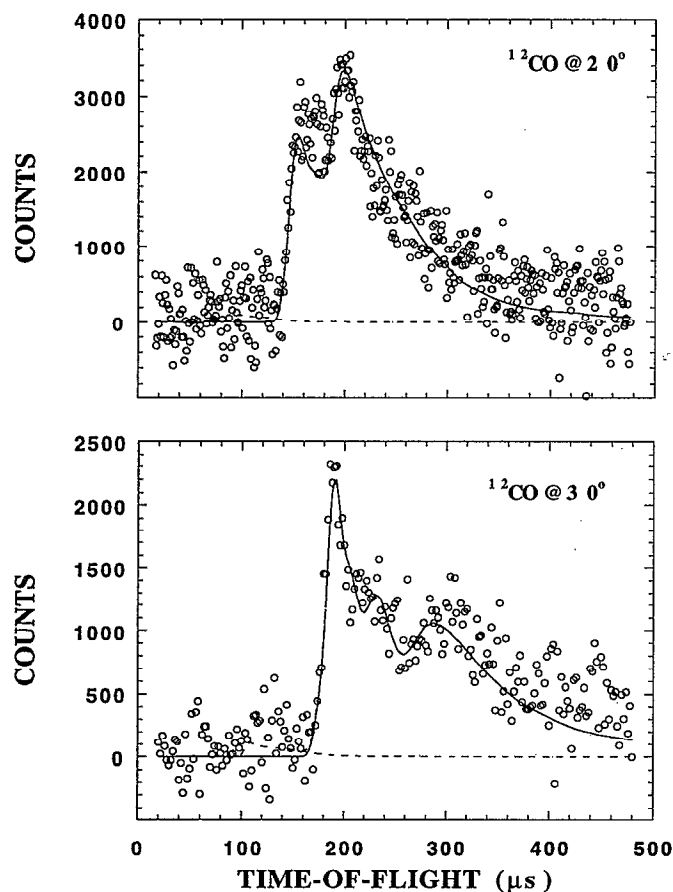


FIG. 10. (top) A time-of-flight distribution at a lab angle of 20° for the ¹²CO fragment from ¹²CO₂ photolysis at 157 nm. (bottom) A time-of-flight distribution at a lab angle of 30° for the ¹²CO fragment from ¹²CO₂ photolysis at 157 nm. Using the $P(E)$ from Fig. 6 for ¹³CO₂ photolysis, we see that the dynamics are not much affected by isotopic substitution.

DISCUSSION

O(³P) channel anisotropy parameter

In order to obtain the O(³P)/O(¹D) electronic branching ratio, the anisotropy parameters, β , must be well known for each channel. The β parameter for O(³P) recoil was suggested to be $\beta=2$ by a fit to a Doppler profile in a collinear pump-probe configuration.⁴ However, as both the anisotropy and the translational energy distribution contribute to the Doppler line shape, it is not possible to unambiguously determine the β parameter with a single pump-probe configuration. The assumption of a *single* O(³P) recoil energy is not a good one. We wondered if the Doppler profile shown in Fig. 3 of Ref. 4 could also be fit with a smaller β parameter and a larger spread of translational energies. Since we measured the translational energy distribution for O(³P) recoil (Fig. 7) we can reconstruct a Doppler line shape for a given choice of β parameter.

In a collinear pump-probe configuration, the Doppler line shape function for a *single* kinetic energy would appear as a rectangle for the case of $\beta=0$ and an inverted parabola for the case of $\beta=2$. In Fig. 7 we have a point-wise representation of the translational energy distribution, $P(E)$, for the O(³P) channel. After transforming $P(E)$ into a veloc-

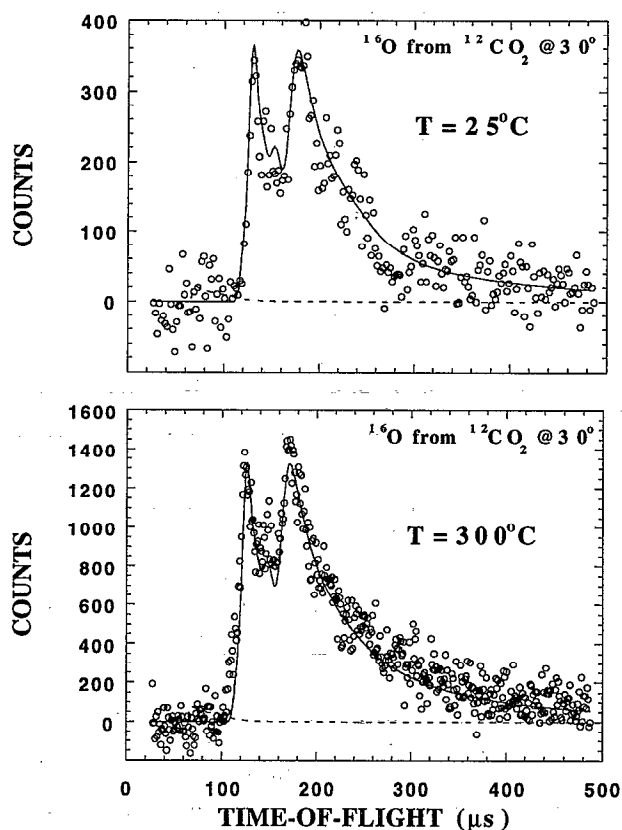


FIG. 11. (top) A time-of-flight distribution at a lab angle of 30° for the ¹⁶O fragment from ¹²CO₂ photolysis at 157 nm with a nozzle temperature of 25 °C. We note that the fit is quite good, indicating that the concentration of hot CO₂($\nu_2=1$) molecule in the fully expanded is close to that at 115 °C. (bottom) A time-of-flight distribution at a lab angle of 30° for the ¹⁶O fragment from ¹²CO₂ photolysis at 157 nm with a nozzle temperature of 300 °C. The fit is not as good, indicating that the concentration of hot CO₂($\nu_2=1$) molecule in the fully expanded is greater than at 115 °C. We note, in particular, that the leading edge of the data is now too fast, indicating a greater contribution from CO₂($\nu_2=1$).

ity distribution $P(v)$, using the Jacobian $E^{1/2}$, we can do a point-wise transformation of the $P(v)$ into a Doppler line shape in order to allow comparison with Fig. 3 of Ref. 4. In the case of $\beta=0$, each point of the $P(v)$ transforms into a rectangle with width proportional to the kinetic energy represented by that point. The overall line shape, therefore, would be a weighted sum of rectangles. In the case of $\beta=2$, each point of the $P(v)$ transforms into an inverted parabola. The overall line shape in this case would be a weighted sum of inverted parabolae.

In order to compare with Fig. 3 of Ref. 4, we consider the case of fine structure transitions originating from the O($2p^3P_{j'}=2$) state. The relative two-photon transition strengths to the O($3p^3P_{j'}$) excited states (where $j'=0,1,2$) have been determined previously.¹²

For the case of $\beta=0$, the derived Doppler line shape (a weighted sum of rectangles) is shown in Fig. 12. For the case of $\beta=2$, the derived Doppler line shape (a weighted sum of inverted parabolae) is shown in Fig. 13. By comparison with the measured Doppler line shape of Ref. 4, retraced in these figures as a narrow solid line, we see that

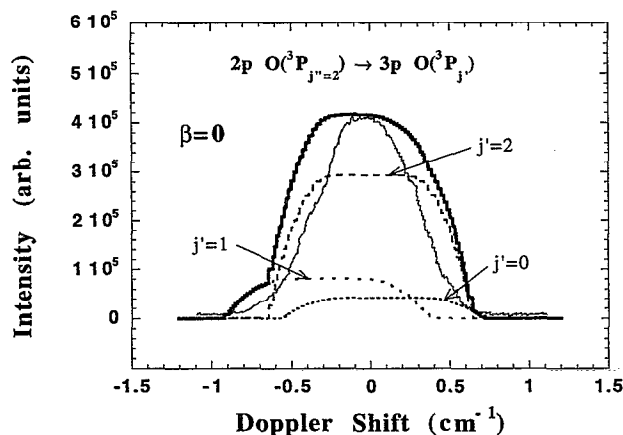


FIG. 12. A Doppler line shape for two-photon $O(^3P_{j'=2})$ detection constructed from the translational energy distribution of Fig. 7 with an anisotropy parameter $\beta=0$. By comparison with Fig. 3 of Ref. 4, retraced here as the narrow solid line, we conclude that the overall linewidth of our construction is too broad, and that the β parameter for the $O(^3P)$ channel must be greater than zero.

the assumption of $\beta=0$ leads to an overall width that is much too broad. By contrast, the assumption of $\beta=2$ leads to an overall width very similar to that in Fig. 3 of Ref. 4. We therefore confirm that the β parameter for the $O(^3P)$ channel should be close to a value of $\beta=2$.

An anisotropy parameter of $\beta=2$ for the spin-forbidden $O(^3P)$ channel is surprising. In contradistinction, an anisotropy parameter of $\beta=0$ was measured for the spin-allowed $O(^1D)$ channel and rationalized on the basis that the molecule bends strongly in the excited state before dissociating. A value of $\beta=2$ for the $O(^3P)$ channel connotes two conclusions. The first is that the $O(^3P)$ channel must arise from a direct transition to an excited triplet state and not from a complex surface-hopping trajectory originating on an excited singlet surface.³ Were the latter

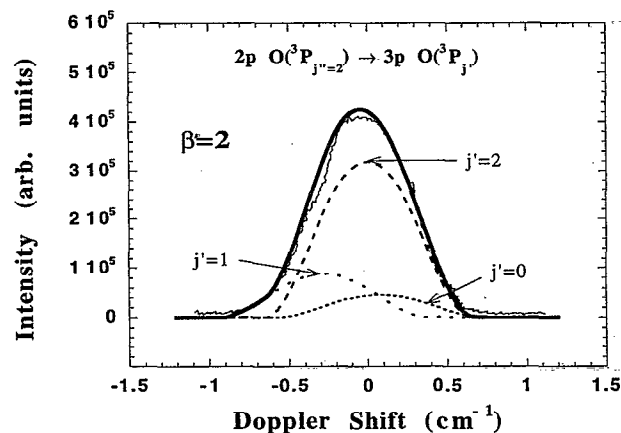


FIG. 13. A Doppler line shape for two-photon $O(^3P_{j'=2})$ detection constructed from the translational energy distribution of Fig. 7 with an anisotropy parameter $\beta=2$. By comparison with Fig. 3 of Ref. 4, retraced here as the narrow solid line, we see that the overall linewidth of our construction is quite similar to the measurement and, therefore, the β parameter for the $O(^3P)$ channel must be close to two.

to be the case, the anisotropy parameter would be the same for both channels—i.e., $\beta=0$. The second conclusion is that the dissociation on the triplet surface must be direct and that the molecule hardly bends during the dissociation. If the molecule were to bend significantly, the β parameter would be reduced from the limiting value of two.

$O(^1D)$ channel assignment

The total $P(E)$ for the $O(^1D)$ channel is shown in Fig. 6. The highest energy peak, near 12 kcal/mol, corresponds to the formation of $CO(v=0)$ from dissociation of the hot $CO_2(v_2=1)$ molecule. This peak is required in order to match the leading edge of the $O(^1D)$ TOF spectrum in Figs. 4 and 5. The second (at 10 kcal/mol) and third (at 8 kcal/mol) highest energy peaks in Fig. 6 correspond to the formation of $CO(v=0)$ from the cold $CO_2(v_2=0)$ molecule: The second arises from the large, narrow feature near 190 μs in Fig. 5, whereas the third arises from the small shoulder near 210 μs . This double-peak structure in Fig. 6 is related to the rotational energy distribution of the $CO(v=0)$ product. This will be discussed below. The fourth peak in Fig. 6 (near 6 kcal/mol), corresponding to the slow, broad shoulder near 240 μs , is due to the formation of $CO(v=1)$ from the hot molecule, $CO_2(v_2=1)$. As can be seen from the Newton diagram of Fig. 3, $CO(v=1)$ product from the cold molecule cannot arrive at the 30° lab angle of Fig. 5.

Referring now to Fig. 4 (10° lab angle), the first shoulder of the $O(^1D)$ TOF spectrum, near 145 μs , originates from the compression of the four above-mentioned peaks in the $P(E)$ of Fig. 6. The largest feature, near 200 μs , corresponds to the formation of $CO(v=1)$ from the cold molecule $CO_2(v_2=0)$, as does the small shoulder near 240 μs time-of-flight. Analogously, the double-peak feature is related to the rotational distribution for $CO(v=1)$ product. This small second peak in the $CO(v=0,1)$ $P(E)$'s would correspond to a maximum at high J in the rotational energy distribution. Such a phenomenon is not unprecedented and has been interpreted in terms of rotational rainbow scattering.¹³ This is plausible since the excited state is known to be strongly bent; furthermore, it is consistent with the measurement of $\beta=0$ for the $O(^1D)$ channel.⁵

Due to the overlap of the peaks in the $P(E)$ of Fig. 6, we are not able to unambiguously obtain vibrational distributions and rotational envelopes for the CO product in the $O(^1D)$ channel. We can, however, compare our results with the full $|v,J\rangle$ product state distributions as given in Ref. 5. This will be discussed in a subsequent section. As a preliminary, we can check our assignment of the peaks in Fig. 6 by artificially dividing the $P(E)$ into three components: (1) a cold molecule $CO(v=0)$, (2) a cold molecule $CO(v=1)$ component, and (3) a hot molecule contribution, as shown in Fig. 14. By assuming rotational distributions for $v=0$ and $v=1$ and a best fit vibrational branching ratio, we can check our assignments. The component-wise fit to the 10° data is shown in Fig. 15 (top), and for 30° (bottom). Although the form of each component $P(E)$ is not unique, they have the constraint that their sum must fit

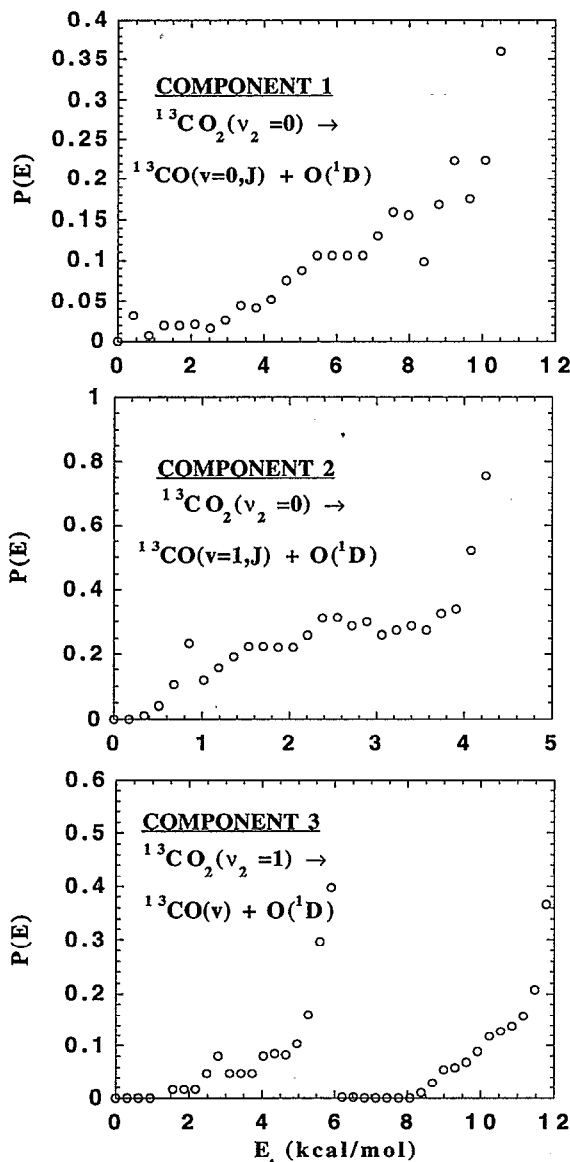


FIG. 14. A decomposition of the overall $P(E)$ for $O(^1D)$ formation of Fig. 6 into components. Although the detailed shape of each $P(E)$ cannot be uniquely determined, their energetic thresholds are very well known and their sum is constrained to be identical to the overall $P(E)$. This helps to assign the various bumps in the overall $P(E)$ of Fig. 6. Shown are $P(E)$'s for the formation of $CO(v=0)$, top, $CO(v=1)$, middle, and a generic hot molecule contribution, bottom.

the data at both angles. As can be seen, the total fit is very good.

The dotted line in Fig. 15 (top) corresponds to the formation of $CO(v=0)$ while the dashed line shows the $CO(v=1)$ product. The dot-dash line shows the hot molecule contribution [forming two peaks, $CO(v=0)$ and $CO(v=1)$]. Any $CO(v=2)$ product, although it may be formed, cannot reach the detector at the lab angles used in these experiments. The hot molecule contribution was assumed to be 10% here. Were it much greater than this, the leading edge of the data would not match. Since the hot molecule peaks do not contribute to the shoulder near 220

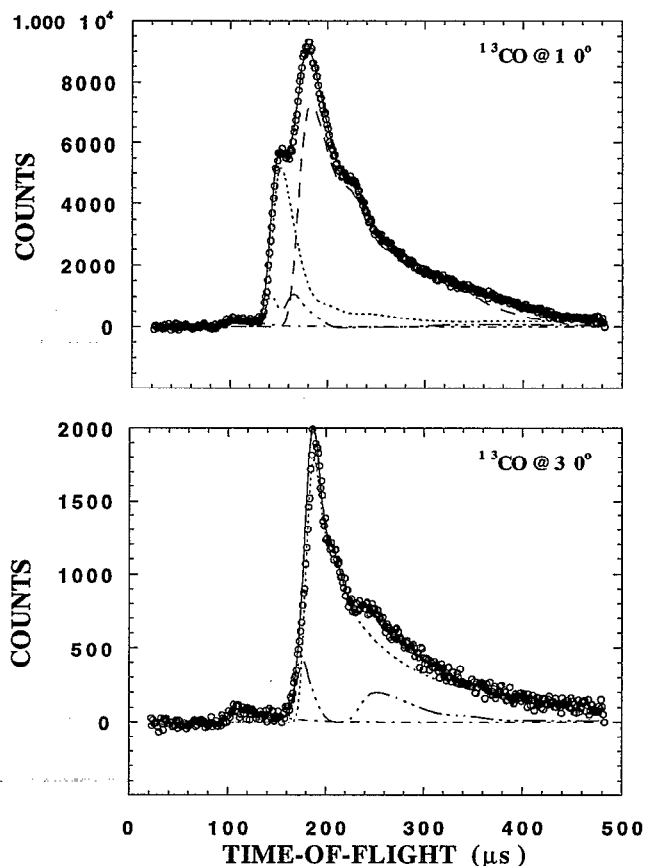


FIG. 15. (top) A component-wise fit using the $P(E)$'s of Fig. 14 at a lab angle of 10° for the ^{13}CO fragment. The dotted line represents $CO(v=0)$, the dashed line represents $CO(v=1)$, and the dot-dash line shows the contribution from the hot molecule. (bottom) A component-wise fit using the $P(E)$'s of Fig. 14 at a lab angle of 30° for the ^{13}CO fragment. Again, the dotted line represents $CO(v=0)$ and the dot-dash line shows the contribution from the hot molecule.

μs in Fig. 15 (top), the shoulder must arise from the specific forms of the rotational envelopes (i.e., the rotational rainbow effect, as discussed in the following section). For the purposes of this simulation, a vibrational branching ratio, $CO(v=0)/CO(v=1)=1.13$ was used. This ratio, however, depends strongly on the assumed forms of the rotational envelopes and cannot, therefore, be taken to be conclusive.

The dotted line in Fig. 15 (bottom) again corresponds to the $CO(v=0)$ product. The $CO(v=1)$ product from the cold molecule doesn't arrive at this angle (see Fig. 3). The hot molecule contribution, the dot-dash line, accounts nicely for both the leading edge of the data [i.e., forming $CO(v=0)$] and the slow shoulder near $240 \mu s$ [i.e., forming $CO(v=1)$].

We conclude that our assignments of the peaks in the $O(^1D)$ $P(E)$ shown in Fig. 6 is reasonable.

$CO(v,J)$ product state distribution

The CO rovibrational product state distributions have been measured by the pump-probe technique using VUV laser induced fluorescence.⁵ The rotational distributions for

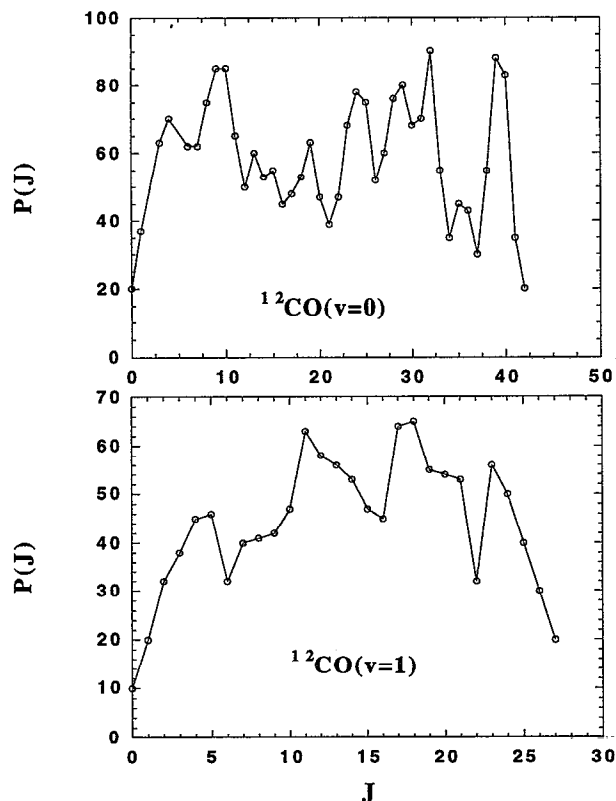


FIG. 16. (top) The rotational distribution for $\text{CO}(v=0)$ in the 157 nm photolysis of CO_2 . (bottom) The rotational distribution for $\text{CO}(v=1)$ in the 157 nm photolysis of CO_2 (from Ref. 5).

the $\text{CO}(v=0)$ and $\text{CO}(v=1)$ product from Ref. 5 are reproduced here in Fig. 16, as (top) and (bottom), respectively. The vibrational branching ratio was measured to be $\text{CO}(v=0)/\text{CO}(v=1) = 3.7 \pm 1.2$. Using these data, due to conservation of energy, we can transform the CO product rovibrational distributions into a product translational energy distribution with which we can compare our time-of-flight data.

We need to transform each rotational energy distribution, $P(J)$, into a translational energy distribution, $P(E)$, and weight each according to the vibrational branching ratio. The sum of these derived $P(E)$'s should fit our data. In order to transform from $P(J)$ to $P(E)$, we must obtain the Jacobian for this transformation:

$$E(J) = BJ(J+1), \quad dE/dJ = B(2J+1), \quad (6)$$

$$P(E)dE = P(J)dJ, \quad P(E) = dJ/dE \times P(J), \quad (7)$$

$$P(E) = P(J)/[B(2J+1)]. \quad (8)$$

The factor, $1/[B(2J+1)]$, is the transformation Jacobian. This is equivalent to assigning all continuum states between J_n and J_{n+1} to the state $|J_n\rangle$. The probability of continuum states, $P(E)$, is therefore weighted inversely by the size of the interval between J_n and J_{n+1} (which increases linearly with J). The result of the transformation of Eq. (8) is shown in Fig. 17 (top) for $\text{CO}(v=0)$ and in Fig. 17 (bottom) for $\text{CO}(v=1)$. It can be seen that, due to the

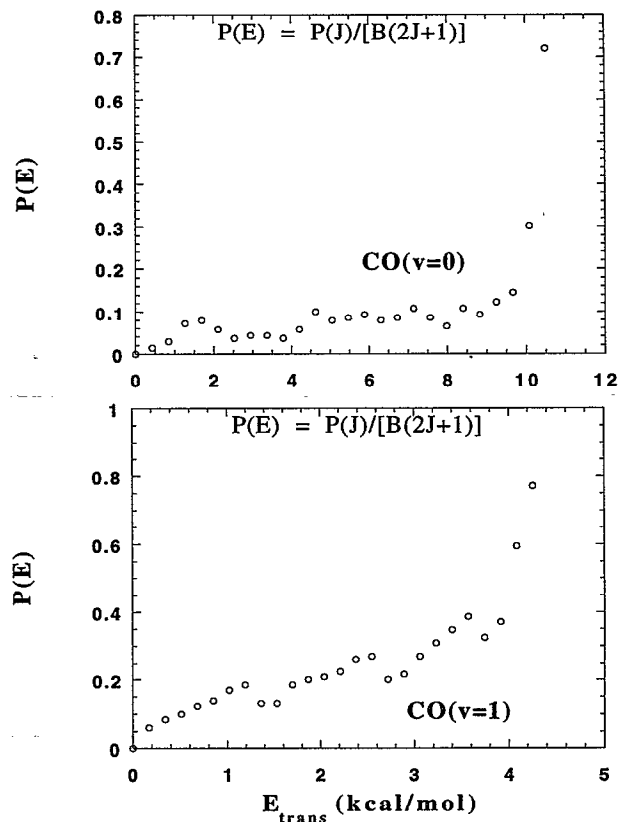


FIG. 17. (top) The transformation, as discussed in the text, of the rotational distribution for $\text{CO}(v=0)$ from Fig. 16 into a translational energy distribution. (bottom) The transformation, as discussed in the text, of the rotational distribution for $\text{CO}(v=1)$ from Fig. 16 into a translational energy distribution.

increasing interval between J_n and J_{n+1} , the high J states contribute much less to the $P(E)$ than the low J states. Using a vibrational branching ratio of 3.7, we can now compare directly with our TOF data without further assumptions.

In Fig. 18 (top), we superimpose the derived $P(E)$'s on our 10° TOF data. The fit is not that good. We note that the $\text{CO}(v=0)$ product, shown as the dotted line, is weighted too heavily. The magnitude of the vibrational branching ratio should be reduced. We can also see how the $\text{CO}(v=0)$ product at large J gives a second peak in the TOF spectrum, as discussed earlier (rotational rainbow). In Fig. 18 (bottom), the derived $P(E)$'s are superimposed on the 30° TOF data. [Only $\text{CO}(v=0)$ arrives at this angle.] It is seen that the rotational envelope for the $\text{CO}(v=0)$ product is too narrow. This may suggest that there is an excess of population in the lowest J states of the pump-probe experiment measured by VUV laser induced fluorescence. Indeed, this was proposed in Ref. 5 and it was speculated that the excess population in the lowest J states originated from CO_2 clusters in the beam. We also note that the leading edge of the 30° data in Fig. 18 is too fast. This is because we have not yet included any contribution from the hot molecule present in our experiment due to our

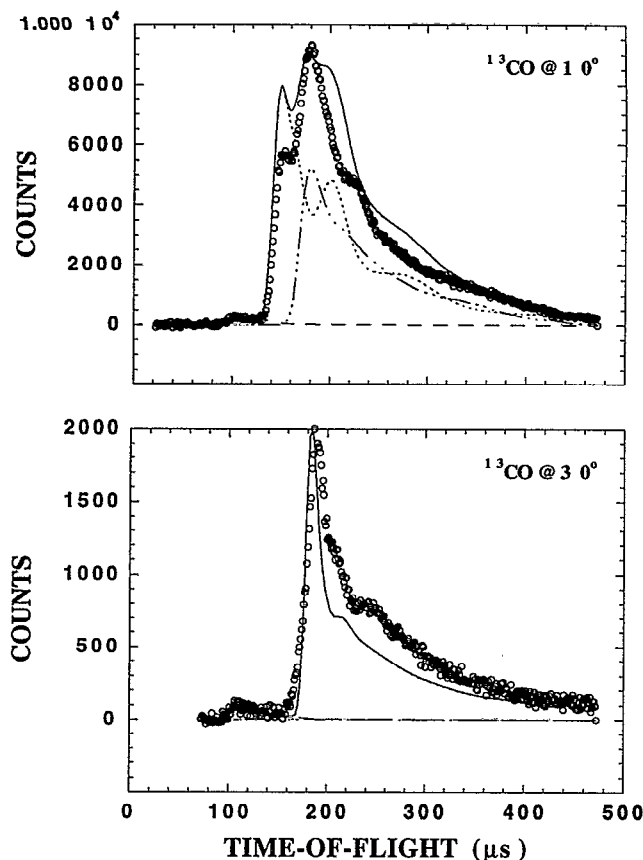


FIG. 18. (top) A fit at a lab angle of 30° for the ^{13}CO fragment from $^{13}\text{CO}_2$ photolysis to the $P(E)$'s from Fig. 17 using a vibrational branching ratio of 3.7 (from Ref. 5). (bottom) The same fit at a lab angle of 10° for the ^{13}CO fragment from $^{13}\text{CO}_2$ photolysis.

heated nozzle. Likewise, the slow shoulder near 240 μs should be accounted for by the hot molecule.

Following the suggestion in Ref. 5 that there is excess population in the very lowest J states, we reduced the weighting of the corresponding two highest energy points in the derived $\text{CO}(v=0)$ $P(E)$ of Fig. 17 (top), leaving all other points unchanged. This "reduced low J " translational energy distribution is shown in Fig. 19 (top). We superimpose this $P(E)$ on our 30° data in Fig. 19 (bottom). The fit is much improved, although the hot molecule contribution is still missing.

In order to obtain our best estimate of the $\text{CO}(v=0)/\text{CO}(v=1)$ vibrational branching ratio for the $\text{O}(^1D)$ channel, we used three channels in the fit: (1) the "reduced low J " $\text{CO}(v=0)$ translational energy distribution of Fig. 19; (2) the unaltered $\text{CO}(v=1)$ translational energy distribution of Fig. 17; and (3) a generic hot molecule contribution as shown in Fig. 14 (bottom). Keeping these forms for the $P(E)$'s, we used a nonlinear least-squares routine to obtain the relative weighting which best fits the data. The best fits are superimposed on the TOF data in Fig. 20, for 10° (top), and for 30° (bottom). With a fit of 13% to the hot molecule contribution, we obtain our best estimate of the vibrational branching ratio, $\text{CO}(v=0)/\text{CO}(v=1) = 1.9$ for the $\text{O}(^1D)$ channel. This is smaller than the

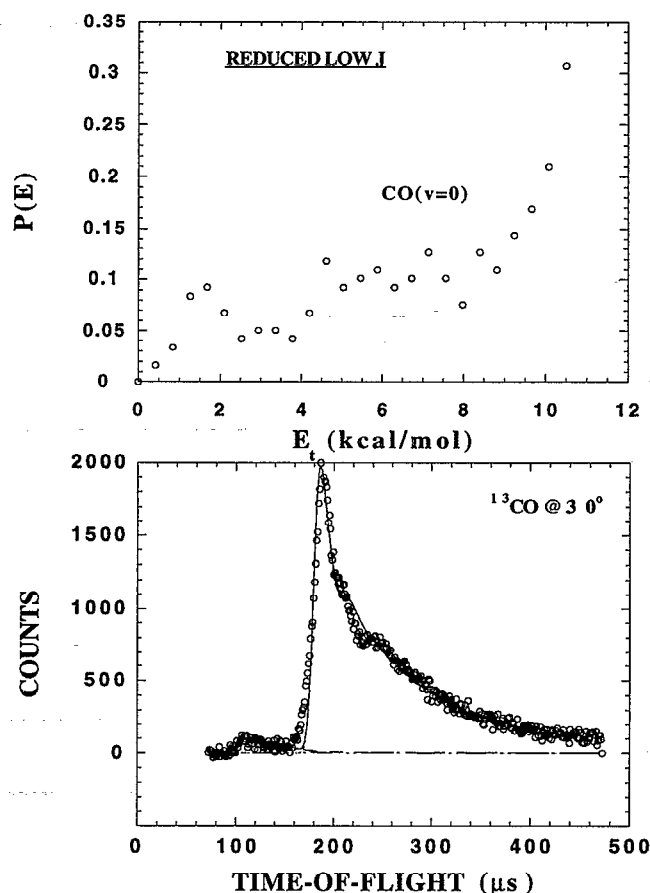


FIG. 19. (top) The probability of two highest energy points in the $\text{CO}(v=0)$ $P(E)$ of Fig. 17 are reduced so as to decrease the effect of the excess population in the lowest J states discussed in the text. All other data points in the $P(E)$ remain unaltered. (bottom) Using the reduced low J $P(E)$ from above, the fit to the 30° data is improved.

lower bound of this branching ratio from the VUV laser induced fluorescence experiment.

CONCLUSION

The photodissociation of $^{13}\text{CO}_2$ at 157 nm was studied by the photofragment-translational spectroscopy technique. The existence of the spin-forbidden $\text{O}(^3P)$ channel was confirmed and a translational energy distribution, $P(E)$, was obtained. A much larger, structured signal, due to the $\text{CO}(v=0,1) + \text{O}(^1D)$ channel, was also observed and a $P(E)$ was obtained, relating to the rovibrational energy distributions in the CO product. The accuracy of the $P(E)$'s was checked by measuring time-of-flight spectra for the momentum-matched ^{16}O recoil partner. The molecule $^{12}\text{CO}_2$ was also studied and it was shown that isotopic substitution does not adversely affect the reaction dynamics. The influence of excitation of the $\text{CO}_2(v_2)$ low frequency bending mode was investigated by varying the temperature of the nozzle and was shown to have a small but not negligible contribution.

With assumptions of $\beta=2$ for the $\text{O}(^3P)$ and $\beta=0$ for the $\text{O}(^1D)$ channel anisotropy parameters, an electronic branching ratio of $6\% \pm 2\%$ $\text{O}(^3P)$ was obtained, agreeing

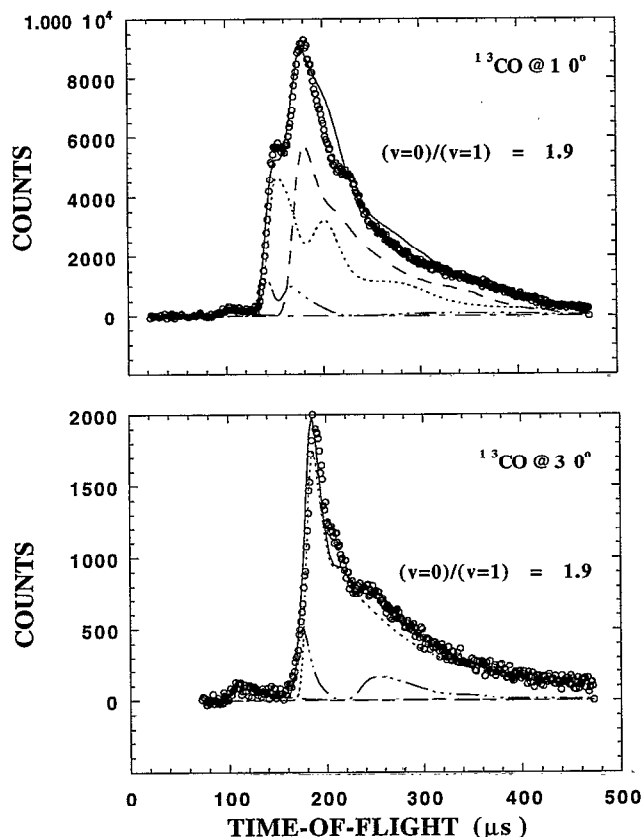


FIG. 20. (top) for 10°. Using the reduced low J CO($v=0$) $P(E)$ from Fig. 19 with the CO($v=1$) $P(E)$ from Fig. 16 and a generic hot molecule contribution as shown in Fig. 14. A least-squares fit yields a 13% hot molecule contribution and our best estimate of the vibrational branching ratio for the O(¹D) channel is CO($v=0$)/CO($v=1$) = 1.9. (bottom) same for 30°.

well with previous results. The translational energy distribution for the CO(v) + O(³P) channel was very broad (over 30 kcal/mol) and appeared to peak near CO($v=0$). The previous determination of the anisotropy parameter for this channel rested upon the unfair assumption of a single recoil energy. We independently confirmed the value of the anisotropy parameter by deriving Doppler line shapes based on our $P(E)$ for two choices of β , namely, 0 and 2. We found that a choice of $\beta=0$ yielded a Doppler linewidth that was much broader than the previously measured line profile of Ref. 4. A choice $\beta=2$ gave a linewidth which compared favorably with that of Ref. 4. We conclude, based on their very different anisotropy parameters, that the O(³P) and O(¹D) products arise from different electronic transitions. Furthermore, the process yielding O(³P) must be a direct dissociation in which the excited molecule hardly bends.

The $P(E)$ for the O(¹D) channel shows considerable structure. Two peaks were identified relating to the formation of CO($v=0$) and CO($v=1$) from the hot CO₂($v_2=1$) molecule. Translational energy distributions for the formation of CO($v=0$) and CO($v=1$) from the cold

CO₂($v_2=0$) molecule were identified and discussed. These distributions showed a secondary feature relating to a maximum in the rotational energy distribution (i.e., rotational rainbow effect). Unfortunately, due to peak overlap, we were not able to unambiguously obtain vibrational branching ratios and rotational envelopes. The assignment of the peaks in the O(¹D) $P(E)$ was checked by constructing a component-wise fit to the overall line shape, based on the well known energetics for the channels.

Product rotational distributions for CO($v=0$) and CO($v=1$), as presented in Ref. 5, were transformed into translational energy distributions to allow for comparison with our TOF data. It was found that the magnitude of the vibrational branching ratio need to be reduced somewhat to fit our data. Furthermore, we suggest that there was an excess of population in the lowest J states for CO($v=0$). Our best estimate of the vibrational branching ratio for the O(¹D) channel is CO($v=0$)/CO($v=1$) = 1.9, smaller than the previously reported value.

We hope that these studies stimulate further investigations into the complex photochemistry of this simple molecule. Detailed *ab initio* studies of nonadiabatic effects in the excited states, including the effect of singlet-triplet interactions, will be valuable.

ACKNOWLEDGMENTS

We thank Lambda-Physik for the generous loan of a VUV excimer laser LPF-205 for these studies. We thank Professor P. L. Houston for permission to reproduce the CO rotational distributions and—along with Professor R. J. Gordon—for helpful discussion. A. S. would like to acknowledge NSERC (Canada) for the receipt of a postdoctoral fellowship. We thank J. D. Myers for a new version of CMLAB and L. Nahon for some plotting software. Some of the equipment used in this experiment was provided by the Office of Naval Research under Contract No. N00014-89-J-1297. This work was supported by the Director, Office of Energy Research, Office of Basic Energy Sciences, Chemical Sciences Division, of the U.S. Department of Energy under Contract No. DE-AC03-76SF00098.

¹T. G. Slanger and G. Black, J. Chem. Phys. **54**, 1889 (1971); **68**, 1844 (1978).

²J. C. Tully, J. Chem. Phys. **61**, 61 (1974); **62**, 1893 (1975).

³Y. F. Zhu and R. J. Gordon, J. Chem. Phys. **92**, 2897 (1990).

⁴Y. Matsumi, N. Shafer, K. Tonokura, M. Kawasaki, Y.-L. Huang, and R. J. Gordon, J. Chem. Phys. **95**, 7311 (1991).

⁵R. L. Miller, S. H. Kable, P. L. Houston, and I. Burak, J. Chem. Phys. **96**, 332 (1991).

⁶R. W. Rabalais, J. M. McDonald, V. Scherr, and S. P. McGlynn, Chem. Rev. **71**, 73 (1971).

⁷P. J. Knowles, P. Rosmus, and H.-J. Werner, Chem. Phys. Lett. **146**, 230 (1988).

⁸R. N. Dixon, Proc. R. Soc. London, Ser. A **275**, 431 (1963).

⁹A. M. Wodtke and Y. T. Lee, J. Phys. Chem. **89**, 4744 (1985).

¹⁰Y. Matsumi and M. Kawasaki, J. Chem. Phys. **93**, 2481 (1990); Y.-L. Huang and R. J. Gordon, *ibid.* **94**, 2640 (1991).

¹¹H. Okabe, *Photochemistry of Small Molecules* (Wiley, New York, 1978).

¹²D. J. Bamford, M. J. Dyer, and W. K. Bischel, Phys. Rev. A **36**, 3497 (1987).

¹³K. Sato, Y. Achiba, H. Nakamura, and K. Kimura, J. Chem. Phys. **85**, 1418 (1986).